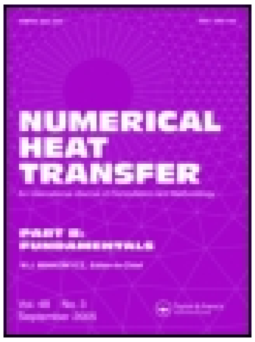

Numerical Heat Transfer, Part B: Fundamentals

An International Journal of Computation and Methodology

ISSN: (Print) (Online) Journal homepage: https://www.tandfonline.com/loi/unhb20

Verification of numerical solutions of thermal radiation problems in participating and nonparticipating media

Antonio Carlos Foltran, Carlos Henrique Marchi & Luís Mauro Moura

NUMERICAL HEAT TRANSFER, PART B: FUNDAMENTALS
https://doi.org/10.1080/10407790.2023.2191871

Verification of numerical solutions of thermal radiation problems in participating and nonparticipating media

Antonio Carlos Foltran[a], Carlos Henrique Marchi[b], and Luís Mauro Moura[c,d]

[a]Graduate Program in Mechanical Engineering (PGMEC), Federal University of Paraná (UFPR), Curitiba, Brazil; [b]Laboratory of Numerical Experimentation (LENA), Department of Mechanical Engineering (DEMEC), Federal University of Paraná (UFPR), Curitiba, Paraná, Brazil; [c]Pontifícia Universidade Católica do Paraná (PUC/PR), Curitiba, Paraná, Brazil; [d]Department of Mechanical Engineering (DEMEC), Federal University of Paraná (UFPR), Curitiba, Paraná, Brazil

ABSTRACT
This article presents an application of the post-processing technique called Repeated Richardson Extrapolation in participating and nonparticipating media problems of radiative heat transfer. It allows us to achieve very accurate results, reducing the estimates of the discretization error of global variables with negligible additional computational time. The error estimates show to be accurate and reliable for code and solution verification. This work also presents equations that quantify the spatial discretization error inside the domain when the Discrete Ordinates Method is used to simulate participating media problems and when basic numerical integration rules are used to solve nonparticipating media problems.

ARTICLE HISTORY
Received 22 August 2022
Revised 9 February 2023
Accepted 9 March 2023

KEYWORDS
Code verification; discrete ordinates method; discretization error equation; Fredholm integral equation; radiative transfer equation; Repeated Richardson Extrapolation; Simpson's 1/3 rule; solution verification; trapezoidal rule; truncation error

1. Introduction

Code verification is a procedure that convincingly demonstrates that a computer code (or at least the exercised part of it) is free of mistakes [1]. Also, according to [1], code verification can be done by checking if the numerical solutions converge to the exact solution at the expected rate in grids of successive refinement ratios. If the formal order-of-accuracy occurs in an asymptotic sense, then the code is considered to be verified for the "exercised" coding options. If not, one suspects the occurrence of code mistakes or implementation errors.

Once a computational code is verified (demonstrated to solve a specific class of problems correctly), the next step is the so-called solution verification, which gives credibility to the numerical results by estimating the discretization error associated with the numerical solution obtained in a specific grid [2–4]. If two or more solutions obtained in different size grids fit in the monotonic convergent region (e.g. the grid element size is small enough that the first term of the discretization error equation is dominant), the error estimates are accurate and reliable.

The analysis of discretization errors in radiative heat transfer is complex because its fundamental variable, the radiation intensity, is dependent not only on space coordinates but also on the direction in which the radiation propagates. Therefore, spatial and angular discretization errors

CONTACT Antonio Carlos Foltran antoniocarlos.foltran@gmail.com Graduate Program in Mechanical Engineering (PGMEC), Federal University of Paraná (UFPR), Av. Cel. Francisco Heráclito dos Santos, Jardim das Américas, 81531-980, Curitiba, Paraná, Brazil.

appear when using a numerical method based on the intensity, for example, the Discrete Ordinates Method (DOM) [5].

This characteristic, which increases the complexity of code verification, justifies the recurrent practice even in high-quality works [6], where comparisons between the solution calculated by the code with solutions found by other numerical methods or programs of recognized credibility occur. However, nothing prevents the occurrence of one or more code mistakes that produce an almost imperceptive error for the tested problem that may influence the results of others with similar mathematical or numerical models.

In the case of problems of nonparticipating media, where nonisothermal surfaces exchange radiation, the energy balance is in the form of a Fredholm integral equation or a system of such equations [7]. For these problems, the spatial discretization error is also present.

This article explores solution verification problems for both participating and nonparticipating media. The following section briefly describes how to estimate the spatial discretization error and the implementation process of the Repeated Richardson Extrapolation (RRE) technique [8–10]. After that, the so-called *a priori* analysis is used to quantify the discretization error when solving Fredholm integral equations (nonparticipating media) and when the DOM is used to solve the Radiative Transfer Equation (RTE) (participating media). Then the results are presented, discussed, and the conclusions pointed out.

2. Discretization error

The numerical error E is given by

$$E(\phi) = \Phi - \phi, \tag{1}$$

where Φ represents the exact analytical solution and ϕ represents its respectively solution obtained numerically in some grid. This definition also can be given by $\phi - \Phi$. In such case, all truncation error equations presented in the following sections of this article need to change the signal to convert between both definitions. If the code does not have programming errors and the round-off and iteration errors are inexistent or very small, then the truncation errors can be grouped in the so called discretization error [11]. In general form, the discretization error equation $E(\phi)$ can be written as [12]

$$E(\phi) = C_0 h^{p_0} + C_1 h^{p_1} + C_2 h^{p_2} + \ldots = \sum_{m=0}^{\infty} C_m h^{p_m}. \tag{2}$$

In Eq. (2), C_0, C_1, ... are coefficients dependent of the derivatives of Φ but independent of the grid element size h. The exponents p_0, p_1, ... are called true orders p_m of the error and assume positive integer values that appears in arithmetical progression, with common difference of successive members $q = p_1 - p_0$. The lower exponent p_0 is called asymptotic order because it dominates the error when $h \to 0$ and the round-off error has not yet been reached, a range called monotonic convergent region. When analyzed in a log versus log graphic, the numerical solutions in this region are situated in a line with inclination p_0, meaning the error is reduced at a rate p_0. As will be mentioned later, when an extrapolation technique is used, higher orders are achieved. The set of all orders are called true orders, given by the following equation, where m is the extrapolation level

$$p_m = p_0 + m(p_1 - p_0), \quad m \geq 0. \tag{3}$$

If the analytical solution of the mathematical model is not yet available, it can be created for a specific problem similar to the one intended to be solved and the asymptotic order can be verified by numerical experiments in grids of successive grid refinement. This technique is called Order Verification Via the Manufactured Solution Procedure (OVMSP) and it is detailed in [1] and [4]. Interestingly, Eq. (2) can be used in cases where the analytical solution is not available. In those cases, it is possible to estimate the discretization error, $U(\phi)$

$$U(\phi) = \phi_\infty - \phi, \tag{4}$$

where ϕ_∞ represents the estimated analytical solution.

There are many error estimators, but in this article only the Richardson U_{Ri} and the Grid Convergence Index U_{GCI} are used [3]. They are calculated by

$$U_{Ri} = \frac{\phi_2 - \phi_1}{r^{p_0} - 1}, \tag{5}$$

$$U_{GCI} = FS\frac{|\phi_2 - \phi_1|}{r^{p_0} - 1}, \tag{6}$$

where $r = h_1/h_2$ is the grid's refinement ratio (constant in this article: $r = 2$), FS is a factor of safety, ϕ_1 and ϕ_2 are the numerical solutions in the coarse and fine grids, respectively. If one does not know if the numerical solutions are outside the monotonic convergence region, it is recommended to use $FS = 3,$ conversely, it is recommended to use $FS = 1.25,$ as in this article. To calculate $U(\phi),$ at least three numerical solutions obtained in grids of successive refinement ratio are required. The linear system formed is solved resulting in Eqs. (5) and (6). Once calculated, the numerical solution with the error estimate is reported as

$$\phi = \phi_2 + U_{Ri(\phi_2)}, \tag{7}$$

$$\phi = \phi_2 \pm U_{GCI(\phi_2)}. \tag{8}$$

When appropriated, an extrapolation method produces, from a certain sequence, a new sequence that converges to the limit of the first one, but with higher order [9]. The Richardson extrapolation can be used as a post-processing technique, increasing the accuracy of results even if low order formulas are employed. It can reduce the discretization error even if the numerical results were obtained in relatively coarse grids, requiring only that these results are already in the monotonic convergence region.

The strategy consists of solving the radiative transfer problem in grids of successive refinement ratio, obtaining, for example, G numerical results of order p_0. These results are then combined to produce $G-1$ extrapolations of order p_1. When comparing the solutions between both sequences in the same grid, the extrapolated result has less error.

Then, this new sequence can be extrapolated again, obtaining a new sequence of $G-2$ extrapolated results of order p_2. This process can be repeated as many times as feasible or desired, sometimes significantly increasing the order of the error. It is not uncommon to reach the round-off error in the last extrapolations. For that reason, all real-type variables in the programs used to obtain the solutions reported in this article are of quadruple precision. The recurrence formula is [12]

$$\phi_{g,m} = \phi_{g,m-1} + \frac{\phi_{g,m-1} - \phi_{g-1,m-1}}{r^{(p_{m-1})} - 1}, \tag{9}$$

valid for $2 \le g \le G$ and $1 \le m \le g-1,$ where g represents the grid number and m the level of extrapolation. The refinement ratio is $r = h_{g-1}/h_g$. It is easy to see that Eq. (9) is the generalization of Eqs. (5) and (7).

Until now, all the true orders p_m are assumed to be known *a priori*, that is, deduced by analysis of the numerical approximations taken to represent derivatives and integrals numerically. However, the orders can be also measured based on numerical results obtained in two successive grids. When the analytical solution is available, one can measure the so called effective order p_E, calculated by [12]

$$(p_E)_{g,m} = \frac{\log\left|\frac{\Phi-\phi_{g-1,m}}{\Phi-\phi_{g,m}}\right|}{\log(r)}, \tag{10}$$

where $2 \le g \le G$ and $0 \le m \le g-2$. If results obtained in many grids are available, then it is expected that $(p_E)_{g,m} \to p_m$ as $h \to 0$.

If the analytical solution is not available, it is still possible to calculate the order by using the results of three successive grids instead of two. Furthermore, if one desires to confirm *a posteriori* the true orders p_m, then Eq. (9) is not entirely independent of the *a priori* analysis, because the extrapolated solutions are based on p_m (in the denominator of Eq. (9)). In such case, it is recommended the use of the so called apparent order or observed order p_U, calculated by [12]

$$(p_U)_{g,m} = \frac{\log\left|\frac{\theta_{g-1,m}-\theta_{g-2,m}}{\theta_{g,m}-\theta_{g-1,m}}\right|}{\log(r)}, \tag{11}$$

valid for $3 \le g \le G$ and $0 \le m \le int[(g-3)/2]$ where *int* meaning the integer part of the result inside the square brackets.

When $m = 0$ the variable θ receives the numerical solution of the radiative transfer problem in its respective grid $\theta_{g,0} = \phi_{g,0}$. Here θ is used to denote extrapolations based on the effective and apparent orders. The extrapolations conducted by using p_U constitute an exclusively *a posteriori* technique. Thus, Eq. (9) is substituted by [12]

$$\theta_{g,m} = \theta_{g,m-1} + \frac{\theta_{g,m-1} - \theta_{g-1,m-1}}{r^{(p_U)_{g,m-1}} - 1}, \tag{12}$$

valid for $3 \le g \le G$ and $1 \le m \le int[(g-1)/2]$. When $h \to 0$, it is expected that $(p_U)_{g,m} \to p_m$. If not, one suspects the occurrence of a hidden programming mistake within the code or a mistake when deducing p_m.

The recursive use of Eq. (9) or (12) constitutes the Repeated Richardson Extrapolation (RRE), a procedure that can be used as a code verification technique. It is important to stress that RRE is employed here to estimate the spatial discretization error, and a general technique, in which both spatial and angular discretization errors are assessed still needs to be developed. The following sections deal with *a priori* analysis of problems of participating and nonparticipating media. After that, the results of the analysis *a posteriori* is presented and discussed.

3. *A priori* analysis of nonparticipating media

Radiative transfer in nonparticipating media is generally described by Fredholm integral equations of the second type. In such problems, two or more nonisothermal surfaces exchange radiation. Depending on the boundary conditions and geometrical disposal, the mathematical models varies from one algebraic equation with one or more integral terms, up to one Fredholm integral equation of the second type or systems of such integral equations.

In general form, an integral equation is given by

$$y(x) - \Lambda \int_a^b K(x,t)y(t)dt = f(x), \tag{13}$$

where K is the kernel (e.g. the exchange factor or the configuration factor) defined in the interval $a \le x \le b$ of the length $L = b - a$, Λ is the characteristic value and f is a term independent of y. The numerical version of Eq. (13) is attained by substituting the integral by a sum

$$y(x)-\Lambda\sum_{k=1}^{N}W_kK(x,x_k)y(x_k)\approx f(x), \tag{14}$$

where W_k are weighting coefficients dependent of the integration rule used. This model substitutes the integral equation by a set of discrete algebraic equations.

In this article two simple integration rules are used in Eq. (14): the trapezoidal rule and the Simpson's 1/3 rule. The deduction of the order of accuracy of such integration techniques is generally due to interpolating polynomials (e.g. Newton-Cotes, Newton-Gregory), but perhaps a more appropriated way to compare this *a priori* result with *a posteriori* results obtained with RRE is by Taylor series expansion, as done in [13, 14] for the discretization of the convective term in CFD problems. The advantage is that not only the asymptotic order is found, but also the following higher orders of accuracy. Therefore, all levels of extrapolated errors or error estimates are checked with this procedure.

The discretization error due to the trapezoidal rule is given by [15, 16]

$$E_L^{trap}=-L\left[\frac{\overline{F^{ii}}}{12}h^2+\frac{\overline{F^{iv}}}{480}h^4+\frac{\overline{F^{vi}}}{53,760}h^6+\dots\right], \tag{15}$$

where h is the grid element size and $\overline{F^{ii}}$, $\overline{F^{iv}}$, and $\overline{F^{vi}}$ represent the arithmetic mean of the second, fourth and sixth derivatives of the integrand over all the domain. More recently, the discretization error equation for the application of the Simpson's 1/3 rule is given by [17]

$$E_L^{Simp}=-L\left(\frac{1}{180}\overline{F_j^{iv}}h^4+\frac{1}{3,780}\overline{F_j^{vi}}h^6+\frac{1}{181,440}\overline{F_j^{viii}}h^8+\dots\right), \tag{16}$$

therefore, in addition to knowing the asymptotic order, this procedure also provides the information that both integration rules have an interval between orders $q=2$. As Eqs. (15) and (16) were demonstrated to quantify the discretization error correctly in the cited works, this is not repeated here.

4. *A priori* analysis of participating media

Several works have been published in the last decades seeking to understand the discretization errors that occur in the DOM [18–21]. Most researchers focus on finding more accurate discretization schemes or mitigating numerical phenomena such as the ray effect and the "false scattering." However, a methodical approach, seeking to quantify the error still needs to be established.

As some basic aspects of the DOM's spatial discretization errors are still undeveloped, it was required to simplify the mathematical model to initiate a comprehensive study, thus this article focuses in the two most basic discretization schemes: the step and diamond schemes. The participating media is considered to be one-dimensional and nonscattering, surrounded by black walls. These simplifications seem to be very restrictive, but they are necessary to isolate errors from different sources and, as shown latter, some more complex problems (scattering in constant-temperature medium) also exhibit true orders consistent with this simple case.

Figure 1 shows a generic volume of length h in a uniform grid. Its nodal point P is situated at the midpoint x_P between the west w and east e faces, positioned at x_w and x_e, respectively.

The Radiative Transfer Equation (RTE) written for this problem is

$$\mu\frac{dI}{dx}+\kappa I=\kappa\hat{I}, \tag{17}$$

where κ is the absorption coefficient of the participating media, I is the directional intensity, μ and is the direction cosine between the discrete ordinate direction $\hat{\boldsymbol{s}}$ and the x axis. The black body intensity of the participating media of temperature T and refractive index n is $\hat{I}=n^2\sigma T^4/\pi$.

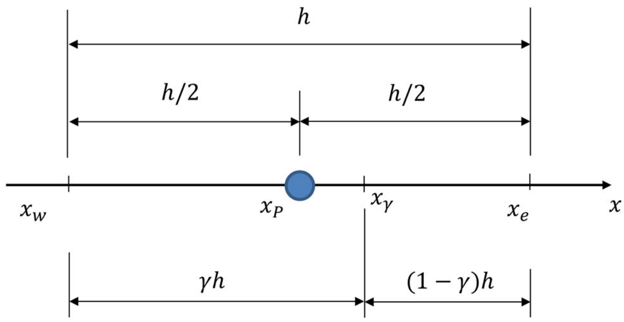

Figure 1. Element of volume at the domain's interior.

Integrating the RTE over an element of volume P gives

$$\mu(I_e - I_w) + \kappa \int_{x_w}^{x_e} I dx = \hat{I}_P h, \tag{18}$$

where I_w and I_e are the intensities at the west and east faces and κ is considered constant in the domain, as also the medium temperature.

In the Discrete Ordinates Method (DOM), the classical spatial weighted approximation is used to link the intensity at the volume center with the intensities at faces

$$I_P \approx \gamma I_e + (1-\gamma) I_w, \ \ 0 < \gamma \leq 1, \tag{19}$$

where γ is the weighting factor. This approximation can be interpreted as a weighted average of the intensity $\bar{I}$ over the volume P, so when the value of I_P is used as average value, as stated by Eq. (19), a truncation error $E_{\bar{I},P}$ is produced

$$\bar{I} = \gamma I_e + (1-\gamma) I_w = I_P + E_{\bar{I},P}. \tag{20}$$

Equation (20) is the one-dimensional version of the approximation, but as multidimensional problems apply weighted averages in each dimension independently of others, the deduction presented here can be extended for two and three dimensions [22]. It is important to point out that in multidimensional problems, increasing the spatial discretization while the angular discretization remains constant can increase the numerical error as a whole, especially if ray effects are present.

Another source of error in Eq. (18) occurs when integrating the intensity over the volume. Using the rectangular rule, the integration results in

$$\int_{x_w}^{x_e} I dx = I_P h + E_{RR,P}, \tag{21}$$

where $E_{RR,P}$ represents the truncation error of the numerical integration. This integration rule also occurs in the term on the right hand side of Eq. (18).

Last of all, and less easy to note is the propagation of the combined truncation errors. It occurs after I_P is calculated, when Eq. (19) is used to extrapolate I_e based on I_P. The combined errors $E_{\bar{I},P}$ and $E_{RR,P}$ are carry out within I_e to the next volume in the process of marching in space because I_e of volume P will be I_w of volume $P+1$ (supposing μ oriented from left to right). Calling this error $E_{e,P-1}$, then I_w should be substituted by $I_w + E_{e,P-1}$ in Eq. (20), given

$$\gamma I_e + (1-\gamma)(I_w + E_{e,P-1}) = I_P + E_{\bar{I},P}. \tag{22}$$

Isolating I_e in Eq. (22) and substituting it together with Eq. (21) in the RTE integrated over the volume Eq. (18), gives

$$I_P = \frac{\mu I_w + \gamma h \hat{I}_P}{\mu + \gamma h\kappa} - \frac{\mu E_{\bar{I},P} + \gamma\kappa E_{RR,P}}{\mu + \gamma h\kappa} + \frac{\mu E_{e,P-1}}{\mu + \gamma h\kappa}, \tag{23}$$

where the first term in the right hand side represent the result of I_P calculated by the DOM and the last two terms constitute its combined truncation errors (i.e. discretization error).

The second term in the right hand side of Eq. (23) combines the truncation errors $E_{\bar{I},P}$ and $E_{RR,P}$ of the volume P and the last term shows how the error $E_{e,P-1}$ from the previous volume $P-1$ is also affected by the weighting process while passing through the volume P. These two terms constitute the discretization error for I_P, and are valid at the central point x_P.

When all sources of numerical error shown here are originated by truncation processes, they are joined together constituting what is called in this article, the discretization error. The discretization error for the volume P is represented by $E_{P,P}$ in Eq. (24), where the first subindex P means the error is calculated at the central nodal point x_P and the second P identifies the index of the volume in the grid. The error coming from the previous volume $E_{e,P-1}$ is discussed in the following paragraphs.

$$E_{P,P} = -\frac{\mu E_{\bar{I},P} + \gamma\kappa E_{RR,P}}{\mu + \gamma h\kappa} + \frac{\mu E_{e,P-1}}{\mu + \gamma h\kappa}. \tag{24}$$

After I_P is calculated with Eq. (23), it is extrapolated with Eq. (22) to find I_e, the intensity exiting the volume P, resulting in

$$I_e = \left(1 - \frac{h\kappa}{\mu + \gamma h\kappa}\right) I_w + \frac{h\hat{I}_P}{\mu + \gamma h\kappa} - \frac{\kappa\left(E_{RR,P} - hE_{\bar{I},P}\right)}{\mu + \gamma h\kappa} + \left(1 - \frac{h\kappa}{\mu + \gamma h\kappa}\right) E_{e,P-1}, \tag{25}$$

where the first and second terms in the right hand side composes the numerical approximation used in the DOM and the third and fourth terms constitute the discretization error $E_{e,P}$ at the east face of volume P.

$$E_{e,P} = -\frac{\kappa\left(E_{RR,P} - hE_{\bar{I},P}\right)}{\mu + \gamma h\kappa} + \left(1 - \frac{h\kappa}{\mu + \gamma h\kappa}\right) E_{e,P-1}, \tag{26}$$

From Eq. (26) it is possible to write a recursive equation for the discretization error from the incident wall back to the point at the boundary where it is emitted

$$E_{e,P} = \prod_{i=P,P-1,\dots}^{1} \left\{ -\frac{\kappa\left(E_{RR,i} - hE_{\bar{I},i}\right)}{\mu + \gamma h\kappa} + \left(1 - \frac{h\kappa}{\mu + \gamma h\kappa}\right) E_{e,i-1} \right\}, \tag{27}$$

where $E_{e,0}$ is the truncation error at the boundary condition. If black walls are at the start of direction $\hat{\mathbf{s}}$, then $E_{e,0} = 0$. If the wall reflects some radiation, then the discretization error exists because the radiation from all directions reaching it is integrated when calculating the incident radiation. In this case, part of it is reflected in the directions exiting the wall. This can have two consequences: a) it is a mechanism by which spatial and angular errors are mixed, even if the medium does not scatter radiation; b) The discretization error equation for the intensity traveling in a specific direction is no longer independent of other directions, instead they constitute a linear system of equations. Those reasons justify the choice of the simplistic mathematical model in this article.

Equation (27) is valid to the east face of volume P, thus can be used to calculate the discretization error reaching the opposite boundary, for example. For calculating the error at some nodal position x_P, Eq. (27) needs to be combined with Eq. (26) leading to

$$E_{P,P} = -\frac{\mu E_{\bar{I},P} + \gamma\kappa E_{RR,P}}{\mu + \gamma h\kappa} + \frac{\mu E_{e,P-1}}{\mu + \gamma h\kappa}, \tag{28}$$

where $E_{e,P-1}$ is given by Eq. (27).

Deducing the weighting average $E_{\bar{I},P}$ and the midpoint rule $E_{RR,P}$ truncation errors that composes Eqs. (27) and (28) is a time consuming task, thus the deductions are given in the Appendices and here only the results are presented and discussed. The weighting average error $E_{\bar{I},P}$ is given by

$$E_{\bar{I}} = F^1_{(\gamma)} I^i_P h + F^2_{(\gamma)} I^{ii}_P h^2 + F^3_{(\gamma)} I^{iii}_P h^3 + F^4_{(\gamma)} I^{iv}_P h^4 + F^5_{(\gamma)} I^{v}_P h^5 + F^6_{(\gamma)} I^{vi}_P h^6 + \ldots, \tag{29}$$

where the function $F^n_{(\gamma)}$ of order n is given by the following formula

$$F^n_{(\gamma)} = \sum_{i=0}^{n} \left\{ \frac{(\gamma - 1/2)^{(n-i)}}{(n-i)!\ i!} \left[(1-\gamma)^i \gamma + (-1)^i (1-\gamma)\gamma^i \right] \right\}, \ n \geq 1. \tag{30}$$

Making $\gamma = 1$ in Eq. (29), the truncation error of the step difference scheme is found

$$E_{\bar{I}} = \frac{I^i_P}{2} h + \frac{I^{ii}_P}{8} h^2 + \frac{I^{iii}_P}{48} h^3 + \frac{I^{iv}_P}{384} h^4 + \frac{I^{v}_P}{3,840} h^5 + \frac{I^{vi}_P}{46,080} h^6 + \ldots, \tag{31}$$

which true orders p_m (i.e. exponents of h) are

$$p_m = 1,\ 2,\ 3,\ \ldots. \tag{32}$$

Making $\gamma = 1/2$ in Eq. (29) the truncation error of the diamond difference scheme is found

$$E_{\bar{I}} = \frac{I^{ii}_P}{8} h^2 + \frac{I^{iv}_P}{384} h^4 + \frac{I^{vi}_P}{46,080} h^6 + \ldots, \tag{33}$$

which true orders p_m are

$$p_m = 2,\ 4,\ 6,\ \ldots. \tag{34}$$

In general, the derivatives in Eq. (29) are expected to be nonnull. One can note that making $\gamma = 1/2$ in Eq. (30) all odd order terms of the series are canceled, making the diamond the only scheme of second order in $[0,\ 1]$ interval. Both Eqs. (32) and (34) are consistent with the well-known asymptotic order observed when weighting schemes are used.

The error due to the single application of the midpoint rule is independent of γ, and given by

$$E_{RR,P} = \frac{I^{ii}_P}{24} h^3 + \frac{I^{iv}_P}{1,920} h^5 + \frac{I^{vi}_P}{322,560} h^7 + \ldots, \tag{35}$$

thus the true orders for this numerical integration rule in a single discrete interval are

$$p_m = 3,\ 5,\ 7,\ \ldots. \tag{36}$$

To test Eqs. (27) and (28), a nonscattering participating medium surrounded by black walls [7] was simulated using the S_6 approximation. The problem is solved in 20 grids of progressive refinement. Considering $L = 1.2\ m$, the grid element size varies from $h = 0.6\ m$ down to $h \cong 1.14 \times 10^{-6}\ m$. The numerical values chosen for the temperatures and absorption coefficient are arbitrary, but values different from 0 and 1 are used (null elements of addition and multiplication, respectively) to test all parts of the code for programming mistakes [1].

The variable analyzed is the directional intensity. Both the analytical Φ and numerical ϕ solutions are calculated with quadruple precision to improve results where $h \to 0$. The numerical error is already known in each grid, and can be compared with Eqs. (27) and (28) with minimum influence of the round-off error E_π. This is done in Figure 2 for the element $P = N$ in the direction with lower μ positive value, but other directions and grid elements behave in the same way. Also the difference between predicted and measured errors, called here ΔE, is presented.

$$\Delta E = E_c - E_m, \tag{37}$$

where E_c and E_m are the calculated and measured errors, respectively.

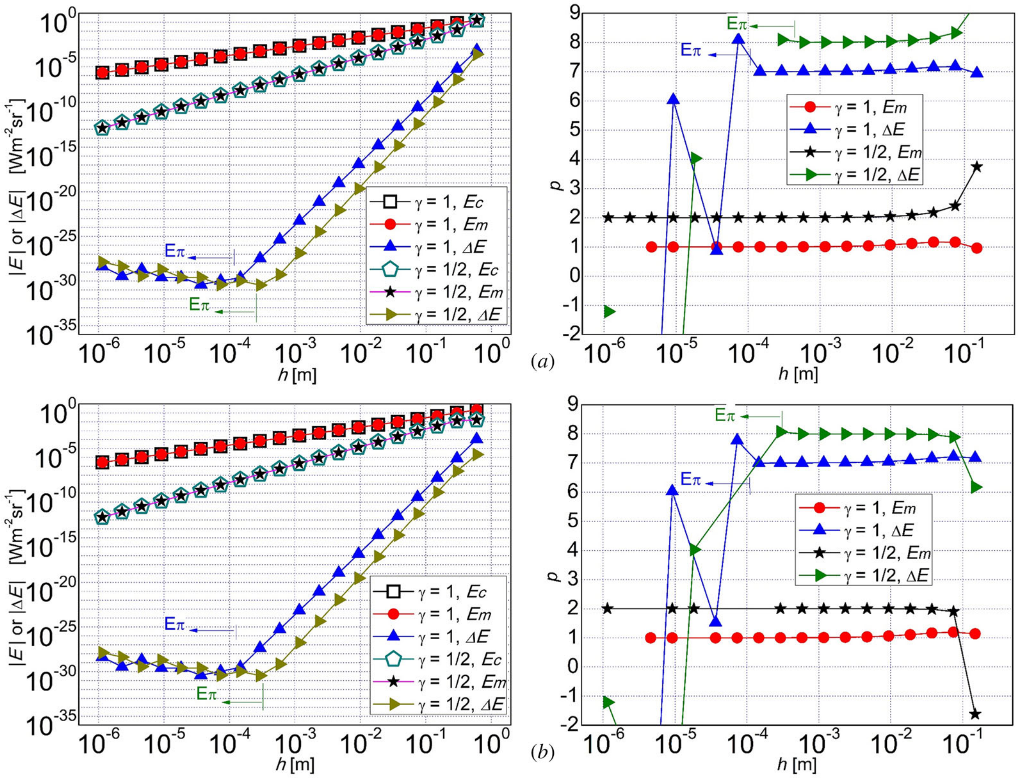

Figure 2. Comparison between calculated and measured discretization errors in radiative intensities and respective apparent order of convergence for (a) $I_P|_{P=N}$ and (b) $I_e|_{P=N}$.

The calculated and measured errors appear to be superimposed for both schemes, as shown in the left side of Figure 2*a*. In the right side of this figure are shown the respective orders of those results. As expected, the apparent order of E_m obtained with the step scheme tends to $p_U = 1$ as $h \to 0$, while the diamond scheme tends to 2. More interesting, the orders of ΔE tends to 7 and 8, respectively. These are the expected orders to be found for ΔE if the three terms deduced in the right hand side of Eqs. (31) and (33) should be correct. Note that the contribution of the midpoint rule, given by Eq. (35), is also tested within this analysis.

The calculated and measured errors of radiative intensity in the most inclined direction ($\mu \cong 0.1839$) are shown in Figure 2*a* for the discretization error in the nodal point P at the volume element N. Figure 2*b* show similar results for the extrapolated value at the point x_e of the volume N. The same behavior was found in all elements of the domain.

This problem has an analytical solution, which is seldom the case, but the error estimate is accurate (within the monotonic convergent region) and available for any problem, although it is not shown in Figure 2 to improve visualization.

5. Results for nonparticipating media

Two problems are presented in this section. The first one is formulated by a system of two Fredholm integral equations of the second kind. The second problem is described by a single Fredholm integral equation. Despite the relative simplicity, the configuration factor inside the equation kernel of the first problem has a noncontinuous first derivative, which degenerates the apparent orders when solving the problem with Simpson's 1/3 rule.

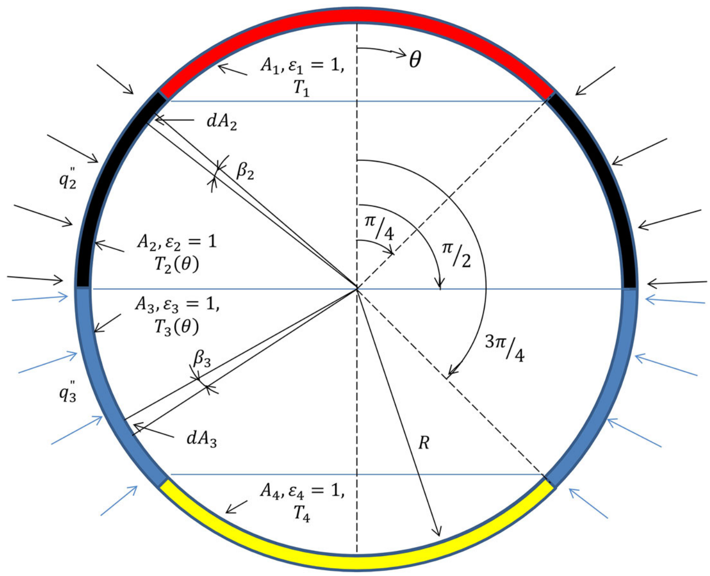

Figure 3. Cavity divided into two spherical caps and two spherical zones.

5.1. System of Fredholm integral equations of the second kind

This problem is proposed by the authors. It consists of a spherical cavity divided into two spherical caps with constant temperature and two spherical zones with prescribed constant heat flux. The surface's nomenclature is shown in Figure 3. The temperatures of the caps are $T_1 = 1{,}000\ K$ and $T_4 = 500\ K$, and the heat fluxes are $q_2'' = 500\ Wm^{-2}$ and $q_3'' = 800\ Wm^{-2}$. The unknowns are the emissive power of the two spherical zones E_2 and E_3.

The mathematical model of this problem is

$$\begin{cases} E_2 - \dfrac{1}{2}\displaystyle\int_{\theta=\pi/4}^{\pi/2} E_2 \sin(\theta) d\theta - \dfrac{1}{2}\displaystyle\int_{\theta=\pi/2}^{3\pi/4} E_3 \sin(\theta) d\theta = q_2'' + (E_1 + E_4)\dfrac{(2-\sqrt{2})}{4} \\ E_3 - \dfrac{1}{2}\displaystyle\int_{\theta=\pi/2}^{3\pi/4} E_3 \sin(\theta) d\theta - \dfrac{1}{2}\displaystyle\int_{\theta=\pi/4}^{\pi/2} E_2 \sin(\theta) d\theta = q_3'' + (E_1 + E_4)\dfrac{(2-\sqrt{2})}{4} \end{cases}, \tag{38}$$

with analytical solution given in Eq. (39) below. As expected by the theory of enclosures, despite the surfaces having different emissive powers (and consequently different temperatures), each value is constant and independent of the polar angle θ.

$$\begin{cases} E_2 = q_2'' + \dfrac{(q_3'' + q_2'')}{2}\dfrac{\sqrt{2}}{(2-\sqrt{2})} + (E_1 + E_4)\dfrac{(2-\sqrt{2})}{4}\left[1 + \dfrac{\sqrt{2}}{(2-\sqrt{2})}\right] \\ E_3 = q_3'' + \dfrac{(q_3'' + q_2'')}{2}\dfrac{\sqrt{2}}{(2-\sqrt{2})} + (E_1 + E_4)\dfrac{(2-\sqrt{2})}{4}\left[1 + \dfrac{\sqrt{2}}{(2-\sqrt{2})}\right] \end{cases}. \tag{39}$$

The error, estimated error, and the effective and apparent orders of E_2 are given in Figure 4. E_3 presents similar characteristics.

Figure 4 presents the classical behavior of the RRE, where $|E|$ and $|U|$ appear as inclined lines, steeper and as the extrapolation level increases. This behavior goes on until a certain point where the round-off error limits the extrapolation process. The round-off error limit is noted for levels $m \gtrsim 4$, where the results turn out to be almost horizontal. It is important to note that this occurs at $|E| \sim 10^{-30}$, therefore compatible with quadruple precision computation of the code we used.

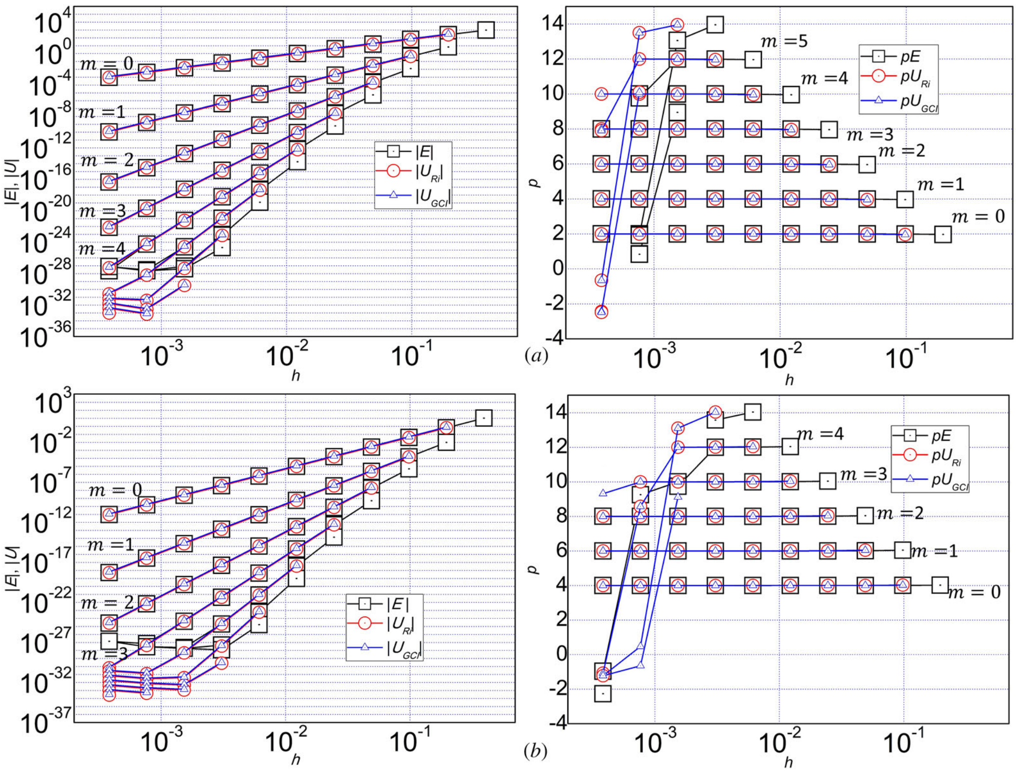

Figure 4. Error, estimated error, and effective and apparent orders for E_2 with (a) the trapezoidal rule and (b) with the Simpson's 1/3 rule.

If double precision were used instead, this limit will be $|E| \sim 10^{-15}$. It is also important to note that the error estimate with both estimators $|U_{Ri}|$ and $|U_{GCI}|$ appears almost superimposed on the error $|E|$, showing the value of this analysis as a tool in solution verification.

In the right side of Figure 4, the effective and apparent orders are presented. They are useful because indicate the rate the error reduces as the grid is refined. As expected, the trapezoidal rule presents the asymptotic order 2 (extrapolation level $m = 0$), while the Simpson's 1/3 rule presents order 4. Furthermore, both integration rules present intervals between subsequent orders $p_m - p_{m-1} = 2$, as predicted by the *a priori* analysis, Eqs. (15) and (16).

This combination of *a posteriori* and *a priori* analysis shows convincingly that the computer code has no mistakes. It enables one to choose one numerical result inside the monotonic convergent region and presented it, with its respective error estimate, as the numerical solution of the problem, as shown in Table 1 for the emissive power and temperatures of surfaces 2 and 3. Despite the analytical values were not shown, they are situated inside the estimated error interval.

5.2. Fredholm integral equation

Despite having a simpler mathematical model than the previous section, the problem analyzed here presents degeneration of some orders when using the Simpson's rule. This is why we presented before the "classical behavior" of RRE and left to show in this section a circumstance that needs care when using RRE and *a posteriori* analysis.

The problem is reported in [23] and consists of a cylindrical enclosure with open ends that receives radiation from its surroundings. This ambient radiation is simulated by hypothetical

Table 1. Numerical results for the $g = 8$ and $m = 4$ with both integration rules.

	Trapezoidal Rule		*Simpson's 1/3 Rule*	
Variable	ϕ [Wm^{-2} or K]	$U_{GCI}(\phi)$	ϕ [Wm^{-2} or K]	$U_{GCI}(\phi)$
E_2	32934.484859279821287	$7.4E-19$	32934.4848592798212866601267	$2.5E-25$
T_2	872.9913220165109083138	$1.5E-21$	872.9913220165109083137492055	$1.1E-27$
E_3	32434.484859279821287	$7.4E-19$	32434.4848592798212866601267	$2.5E-25$
T_3	869.6589264665268396797	$1.5E-21$	869.6589264665268396796721292	$1.1E-27$

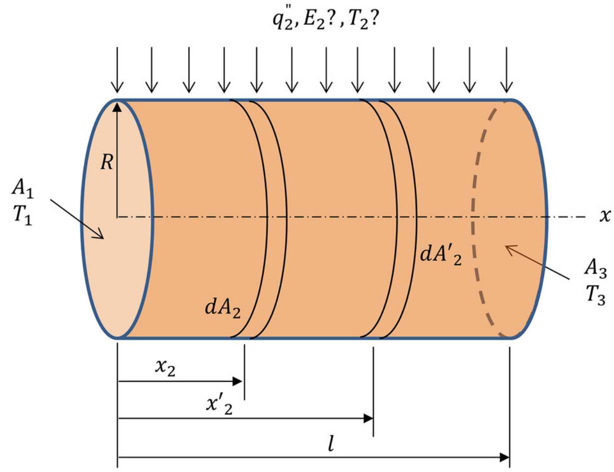

Figure 5. Dimensions of the cylindrical enclosure with constant heat flux in the lateral area and open ends to surrounding radiation.

circular surfaces with black body temperature compatible with the radiation from the surrounding, as shown in Figure 5.

The mathematical model for the emissive power of the lateral area is the following Fredholm integral equation

$$E_2(X_2) - \int_0^{X_2} E_2(X_2)K(X_2, X'_2)dX_2 - \int_{X_2}^{L} E_2(X_2)K(X_2, X'_2)dX_2$$
$$= q''_2 + \sigma T_1^4\left[\frac{X_2^2 + {}^1/_2}{\sqrt{X_2^2+1}} - X_2^2\right] + \sigma T_3^4\left[\frac{(L-X_2)^2 + {}^1/_2}{\sqrt{(L-X_2)^2+1}} - (L-X_2)^2\right], \tag{40}$$

where the coordinates have been made nondimensional by $X_2 = \frac{x_2}{2R}$, $X'_2 = \frac{x'_2}{2R}$ and $L = \frac{l}{2R}$. The kernel of the integral $K(X_2, X'_2)$ is the configuration factor (exchange factor) between two infinitesimal area elements, given by

$$K(X_2, X'_2) = 1 - \frac{Z^3 + \frac{3}{2}Z}{\sqrt{Z^2+1}}, \quad Z = |X_2 - X'_2|. \tag{41}$$

The configuration factor related to the radiation incoming from the surroundings K_e is given by

$$K_e(S) = \frac{S^2 + \frac{1}{2}}{\sqrt{S^2+1}} - S^2, \tag{42}$$

were $S = \frac{x_2}{2R}$ or $S = \frac{l-x_2}{2R}$ depending on what extremity is evaluated.

The error and error estimate for $T_2(X_2 = 0)$ is presented in Figure 6. Similar behavior was found for T_2 in other positions along with the interval $[0, L]$.

As the analytical solution of Eq. (40) is approximated, it is expected that the error and its estimated value will agree only in the coarsest grids and extrapolation level $m = 0$. Besides that, in Figure 6*a*, the expected behavior of RRE is found for the application of the trapezoidal rule, with expected asymptotic order and interval between orders.

Conversely, when using the Simpson's 1/3 rule, the asymptotic order degenerates (2 instead of 4). In addition, subsequent extrapolations levels are ineffective in increasing the order. It is expected, because the configuration factor function has discontinuous derivative. As the Simpson's rules swept the domain every two discrete intervals when $Z = 0$ in one of these two intervals, the derivative has different values in each interval, and Eq. (13) presented in [17] loses its validity. This does not happen when using the trapezoidal rule because it sweeps the discrete intervals one by one.

A strategy to deal with this problem is substituting the configuration factor with a similar smooth function and solving the problem and doing RRE. Obviously, the solved problem will not be the same, but the difference between the solutions is small, and, more important, the code can be verified comparing the analysis *a priori* and *a posteriori*.

6. Results for participating media

This section describes three problems, from the simple absorbing-emitting medium with constant temperature, passing to a more complex problem, where scattering is also present (despite *a priori* analysis does not consider scattering), and ending with the radiative equilibrium problem.

6.1. Absorbing-emitting medium with constant temperature

The test problem consists of a unidimensional domain filled with an absorbing-emitting medium of constant absorption coefficient $\kappa = 4.0\ m^{-1}$, length $L = 0.5\ m$, maintained at $T = 2,000\ K$. Both boundary walls are black and maintained at $T_w = 400\ K$. The S_8 angular approximation is used. The problem is solved in 18 grids of progressive refinement ratio, thus considering the value assumed for L, the size of the element of volume varies from $h = 0.25\ m$ down to $h \cong 1.91 \times 10^{-6}\ m$.

Due to the simplicity of this problem, all variables analyzed have an analytical solution. They are: a) intensity in the more inclined discrete direction related to the x axis $I_e(\mu \cong 0.142)$; b) idem, but in the less inclined direction $I_e(\mu \cong 0.979)$; c) heat flux at the east wall q''_e; d) irradiation over the east wall H_e; and e) incident radiation at the center of the domain $G_{L/2}$.

The error, estimated error, and the orders (effective and apparent) for $G_{L/2}$ using both the step and diamond schemes are given in Figure 7.

Graphically, the error estimate appears to be coincident with the respective error, except for the higher levels of extrapolation, again displaying the capability of RRE for achieving very accurate results, reaching $|E| \sim 10^{-24}$. The effective and apparent orders found *a posteriori* corroborate those deduced *a priori* in this article: $p_m = 1,\ 2,\ 3,\ \ldots$ for $\gamma = 1$ and $p_m = 2,\ 4,\ 6,\ \ldots$ for $\gamma = 1/2$. Despite only results for $G_{L/2}$ being shown, all the other variables analyzed present similar graphics.

The analytical results are shown in Table 2 with 35 significant digits for proper comparison with numerical results. Tables 3 and 4 show, respectively, the numerical results related to $g = 18$ and $m = 5$ for the step scheme and $g = 12$ and $m = 4$ for the diamond scheme. The criteria used to select those specific grids (g) and extrapolation levels (m) is the most accurate result considering all variables of the problem using each scheme.

Closing this section, we report that a preliminary study of an absorbing-emitting medium of variable temperature also presents apparent orders as predicted in this article, except for the incident radiation in the center of the domain $G_{L/2}$, which present $p_m = 1,\ 2,\ 3,\ \ldots$ for both $\gamma = 1$

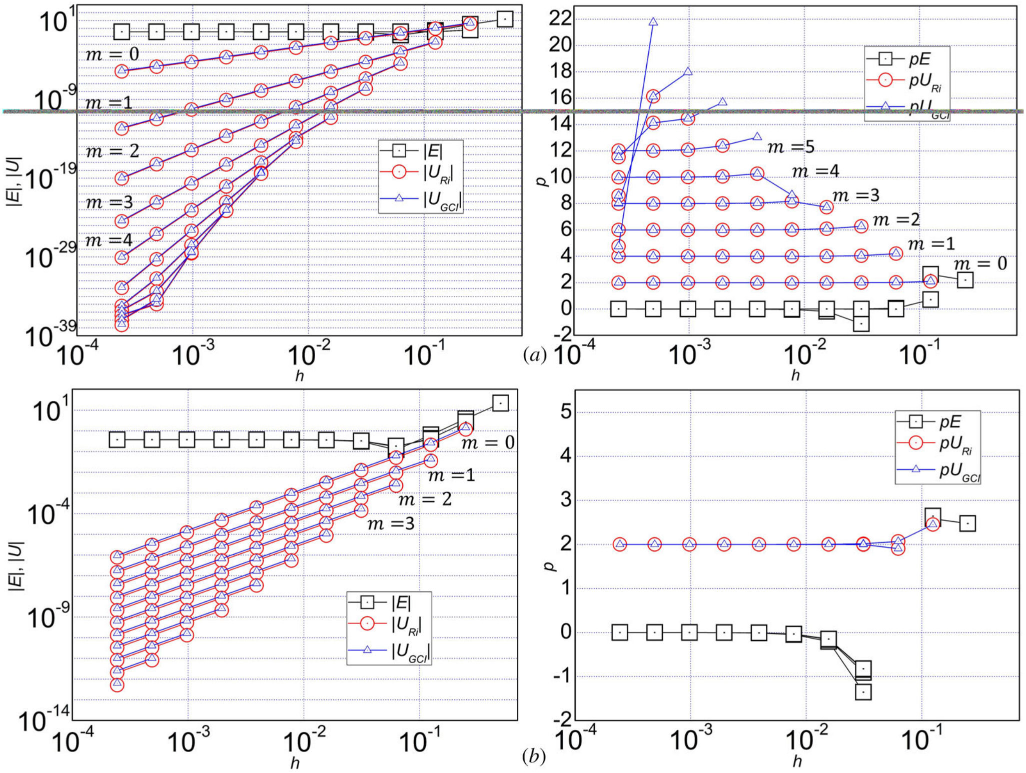

Figure 6. Error, estimated error, and effective and apparent orders for the finite length tube are solved with (a) the trapezoidal rule and (b) the Simpson's 1/3 rule.

and $\gamma = 1/2$. A possible explanation for this behavior is the integration of the source term, where a truncation error due to the rectangle rule is recognized but not investigated in this article. Another explanation is because this variable is calculated as a weighted sum, and a simplification of h can occur. In the radiative equilibrium problem, $G_{L/2}$ also behaves this way, as will be shown later.

6.2. Absorbing, emitting, and scattering medium of constant temperature and pure scattering medium problems

With the knowledge gained from the *a priori* analysis, it is time to consider adding isotropic scattering to the mathematical model. The scattering should not produce a new source of spatial truncation error. Instead, it only redirects a parcel of this error from one direction to another. Thus the error equation is expected to give place to a system of error equations. As shown in this section, adding isotropic scattering to the model (maintaining the temperature constant), the true orders deduced *a priori* for a constant-temperature absorbing-emitting medium remain the same.

Two cases are studied. First, a medium that absorbs emits and scatters radiation with $\kappa = 2.0\ m^{-1}$ and a scattering coefficient $\sigma_s = 2.0\ m^{-1}$ (corresponding to a scattering albedo $\omega = 0.5$). The second is the pure scattering problem with $\sigma_s = 4.0\ m^{-1}$. In both cases, the medium has a constant temperature $T = 2,000\ K$ and it is surrounded by black walls at $T_w = 400\ K$. The domain's length is $L = 0.5\ m$. The problem is solved with the S_6 approximation in 14 grids with h varying from 0.25 down to $3.1 \times 10^{-5}\ m$.

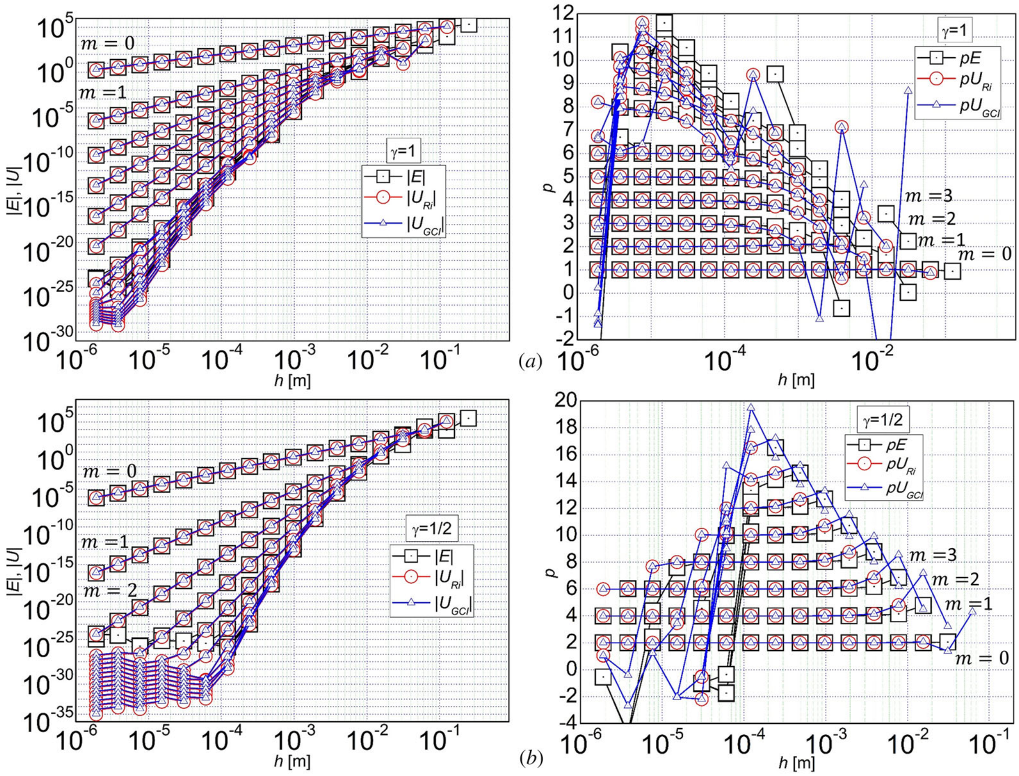

Figure 7. Error, estimated error, and effective and apparent orders for $G_{L/2}$ in the absorbing-emitting medium with constant temperature (a) for $\gamma = 1$, (b) for $\gamma = 1/2$.

Table 2. Analytical solutions of the variables analyzed in the absorbing-emitting medium problem with a constant temperature.

Variable	Φ
$I_e(\mu \cong 0.142)$ $[Wm^{-2}sr^{-1}]$	2.8878919393370874256338668412526899E + 05
$I_e(\mu \cong 0.979)$ $[Wm^{-2}sr^{-1}]$	2.5136394624083471267025473008156992E + 05
q''_e $[Wm^{-2}]$	8.5164205345700896093007704746407975E + 05
H_e $[Wm^{-2}]$	8.5309366740900896093007704746407980E + 05
$G_{L/2}$ $[Wm^{-2}]$[a]	3.0842452650698763813282973016904239E + 06

[a]Calculated based on the solution of the S_8 approximation instead of the RTE.

Table 3. Numerical solutions of the variables analyzed in the absorbing-emitting medium problem of a constant temperature with RRE ($\gamma = 1,\ g = 18,\ m = 5$).

Variable	ϕ $[Wm^{-2}sr^{-1}$ or $Wm^{-2}]$	$U_{GCI}(\phi)$
$I_e(\mu \approx 0.1)$	2.88789193933708742563386683 60E + 05	6.6E-22
$I_e(\mu \approx 0.9)$	2.51363946240834712670254730 0930E + 05	8.7E-24
q''_e	8.516420534570089609300770 4735E + 05	1.6E-22
H_e	8.530936674090089609300770 4735E + 05	1.6E-22
$G_{L/2}$	3.084245265069876381328297266E + 06	4.5E-20

Table 4. Numerical solutions of the variables analyzed in the absorbing-emitting medium of a constant temperature problem with RRE ($\gamma = 1/2,\ g = 12,\ m = 4$).

Variable	ϕ $[Wm^{-2}sr^{-1}$ or $Wm^{-2}]$	$U_{GCI}(\phi)$
$I_e(\mu \approx 0.1)$	2.8878919393370874256338668 4099E + 05	3.3E-23
$I_e(\mu \approx 0.9)$	2.5136394624083471267025473008152E + 05	8.0E-28
q''_e	8.5164205345700896093007704 7456E + 05	1.0E-23
H_e	8.5309366740900896093007704 7456E + 05	1.0E-23
$G_{L/2}$	3.084245265069876381328297288E + 06	1.8E-20

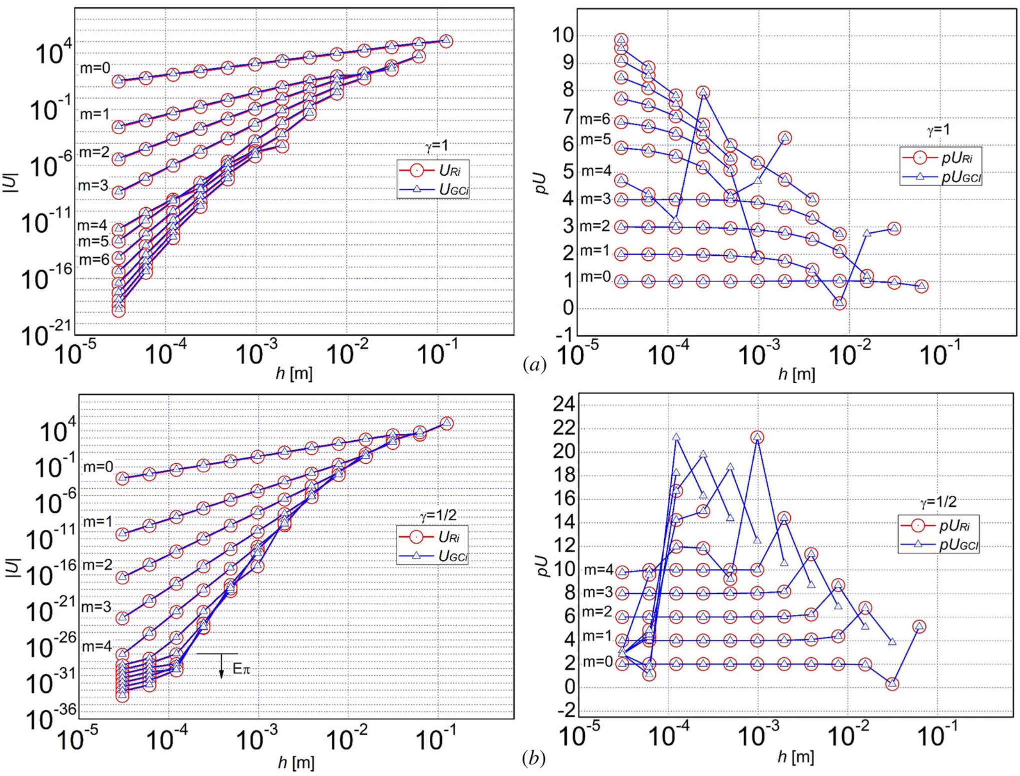

Figure 8. Estimated error and apparent order for $G_{L/2}$ in a medium of constant temperature that absorbs, emits, and scatters radiation, (a) for $\gamma = 1$, (b) for $\gamma = 1/2$.

The same variables of the previous section were analyzed, but as any one presented anomalies in the predicted true orders, only $G_{L/2}$ is shown in Figure 8 for the first case and in Figure 9 for the second. The only distinct feature is in Figure 8*a*, where the data for $m = 4$ appears to present an infinite jump in the range $10^{-3} < h < 10^{-4}$, but this feature is commonly found when the apparent order is calculated in CFD studies, even without conducting RRE as shown in the page 336 of [2] or in [24].

6.3. Radiative equilibrium problem

The difference between this problem and those from the previous section is the need of running the DOM iteratively, actualizing the medium temperature and emission term until they converge to some constant value. The new temperature field is obtained by

$$T_P = \sqrt[4]{\frac{G_P}{4\sigma}}, \tag{43}$$

where the incident radiation G at the discrete volume P is given by

$$G_P \cong \sum_{k=1}^{nd} w^k I_P^k. \tag{44}$$

Equation (44) shows the coupling between spatial and angular discretization errors, where nd is the number of directions. Despite this coupling, all variables studied in Table 2 were analyzed in this section. The medium temperature at the middle of the domain $T_{L/2}$ is also included. As

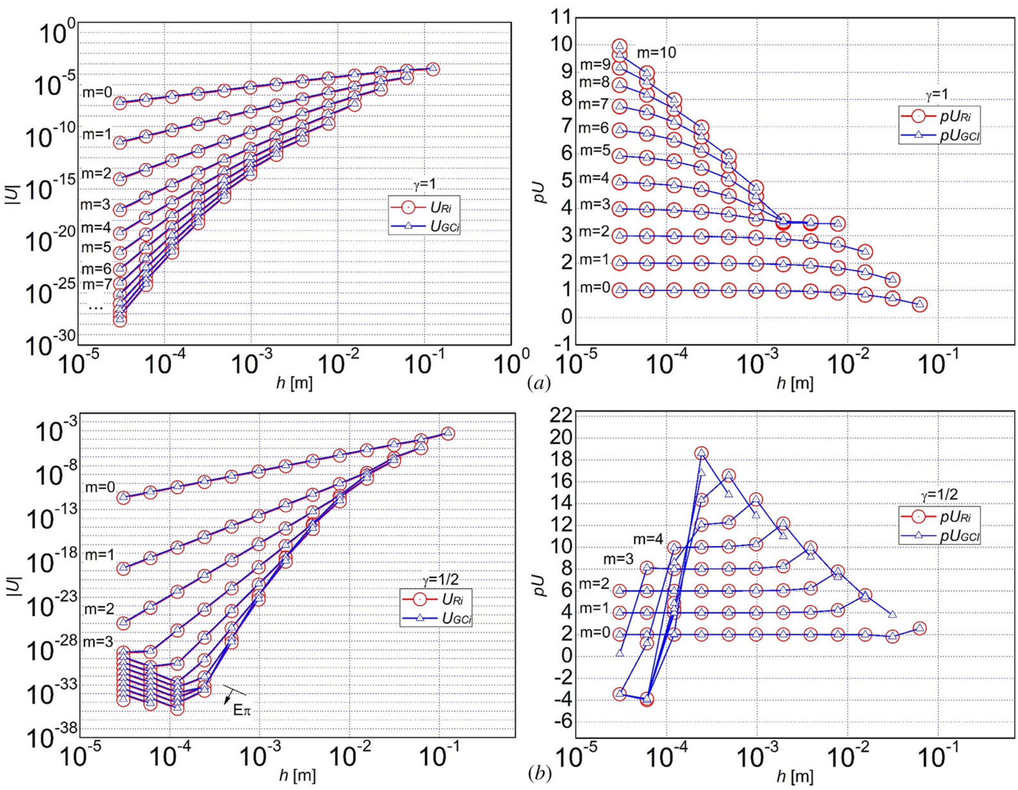

Figure 9. Estimated error and apparent order for $G_{L/2}$ for the pure scattering problem, (a) for $\gamma = 1$, (b) for $\gamma = 1/2$.

expected, only $G_{L/2}$ and $T_{L/2}$ presented *a posteriori* orders that do not agree with the analysis *a priori* reported in this article.

The domain consists of a participating medium with $\kappa = 0.9\ m^{-1}$, $\sigma_s = 0.4\ m^{-1}$ and $L = 1.3\ m$ (optical thickness, $\tau = \beta L = 1.69\ m^{-1}$), maintained in radiative equilibrium with its boundaries, that are black walls maintained at $T_0 = 500\ K$ and $T_L = 1,000\ K$.

The problem is solved with the S_2 approximation in 12 grids, with h in the range between $h = 0.65\ m$ and $h \cong 3.2 \times 10^{-4}\ m$. As this problem is solved iteratively, the stop criteria play a role in the accuracy of results. We used the L^1 norm of the residue of intensity, accounting for all discrete volumes and all directions. Its value is normalized by dividing it by its value at the first iteration. When the value becomes lower than 10^{-30}, the iterative process stops (it requires 388 iterations and 41 s CPU time in a 1.6 GHz Intel R Pentium processor and a 4.0 GB memory).

As stated before, all variables corroborate the true orders deduced *a priori*, except for $T_{L/2}$ and $G_{L/2}$, whose results are presented in Figures 10 and 11, respectively. The analytical solution for $T_{L/2}$ used in this article is approximated [25], thus the error remains almost constant below 10^{-6} and $p_E \to 0$ for $h \lesssim 10^{-2}\ m$, but for $h \gtrsim 10^{-2}\ m$ Figure 10 shows that $|E|$ and $|U|$ curves agree very well each other. One can note that $\gamma = 1/2$ results behave normally, but $\gamma = 1$ has its asymptotic order increased for $p_0 = 2$ and preserves its interval between orders $q = 1$.

The incident radiation $G_{L/2}$ presents asymptotic order $p_0 = 1$ and interval between orders $q = 1$ for both schemes $\gamma = 1$ and $\gamma = 1/2$. We guest two possible contributing factors to explain the behavior of these two variables: the interaction of spatial errors with errors due to the angular approximation or during the integration of the source term $\hat{I}$ (because T is no more a constant valued function). Whatever the cause, the other variables presented the true orders predicted by the *a priori* analysis for participating media maintained at a constant temperature.

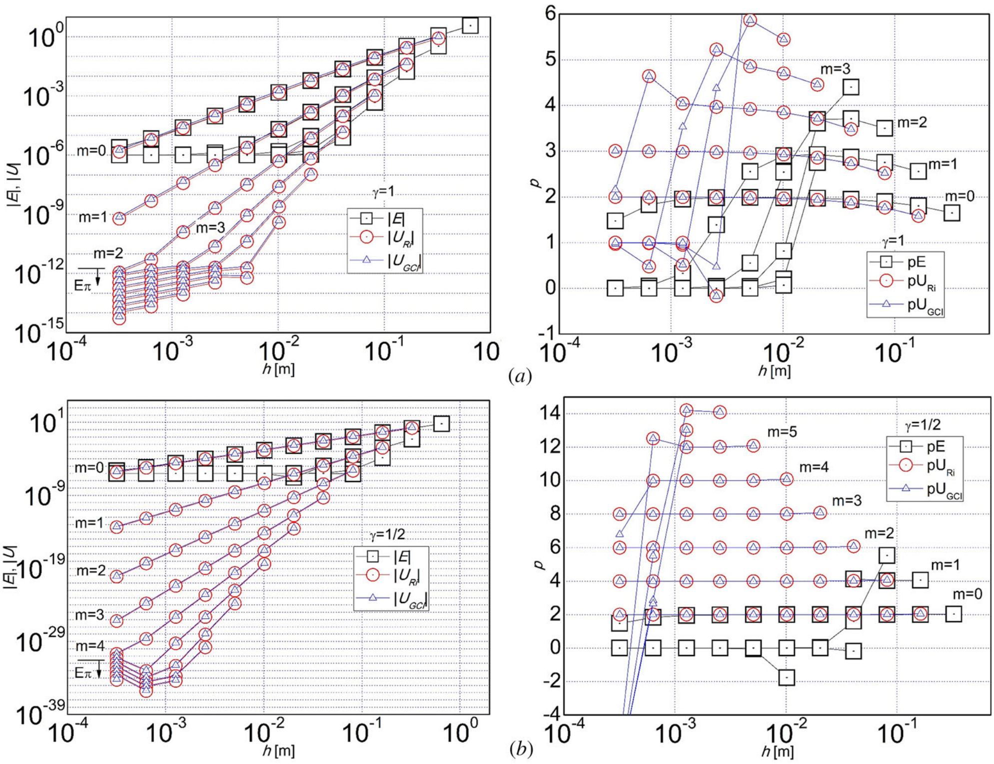

Figure 10. Error, estimated error and effective and apparent orders for $T_{L/2}$ for the radiative equilibrium problem, (a) for $\gamma = 1$, (b) for $\gamma = 1/2$.

7. Conclusions

In this article are deduced spatial discretization error equations for some numerical models used to describe both participating and nonparticipating media problems of thermal radiation. Those equations predict the orders of the discretization error, constituting an *a priori* analysis.

The application of the Repeated Richardson Extrapolations is not exclusively a technique to improve the accuracy of results and estimate the discretization error. But it also contributes as a code verification tool, allowing to measure, *a posteriori*, the orders of the spatial discretization error. The Richardson estimator and the Grid Convergence Index (GCI) are applied to estimate the discretization error. Both were suitable for the analyzed radiative transfer problems. Once two different classes of problems exist, conclusions are separated accordingly in the following topics.

7.1. Nonparticipating media problems

Generally modeled by Fredholm integral equations, nonparticipating media problems can be solved by the trapezoidal and the Simpson's rules, resulting in linear systems with nonsparse matrices. Based on the Finite Difference Method, the already known discretization error equation is used for both the trapezoidal and the Simpson's 1/3 rules as an *a priori* analysis of the problems. Two problems are analyzed: a single Fredholm integral equation (with discontinuous first derivative) and a system of two Fredholm integral equations of the second kind.

In addition to the well-known asymptotic order $p_0 = 2$, *a posteriori* results show that, when submitted to RRE, the trapezoidal rule has interval between orders $q = 2$ constituting the set $p =$

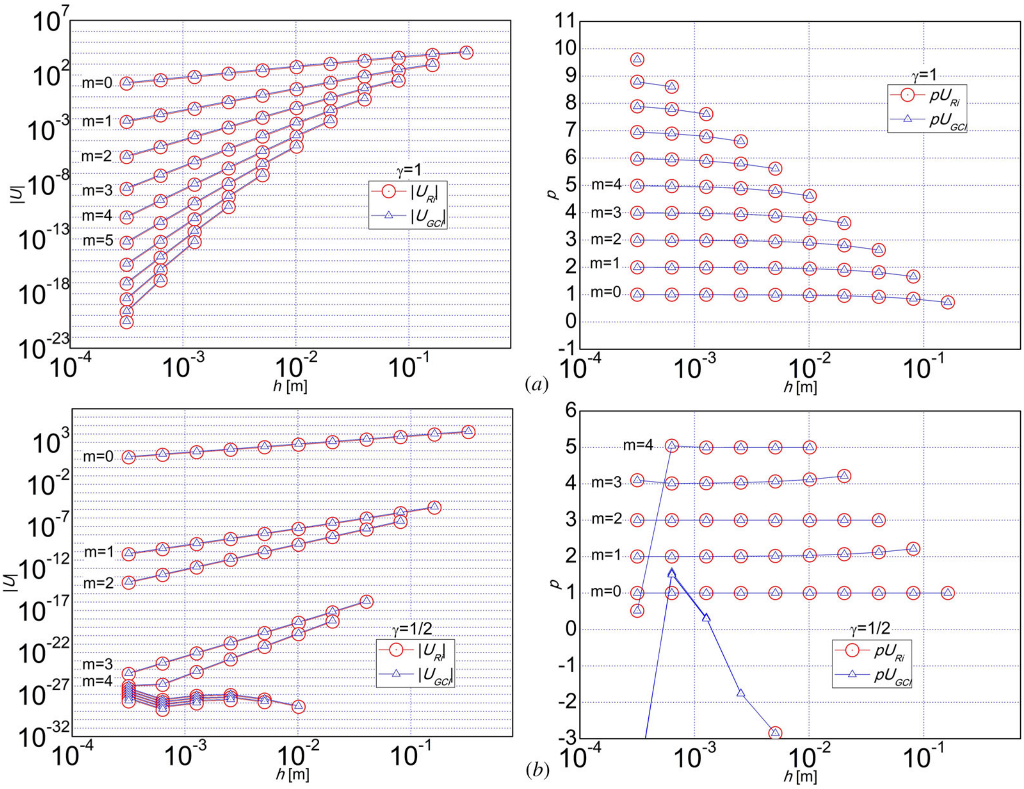

Figure 11. Error, estimated error, and apparent order for $G_{L/2}$ for the radiative equilibrium problem, (a) for $\gamma = 1$, (b) for $\gamma = 1/2$.

$(2, 4, 6, \ldots)$. The equivalent for the Simpson's 1/3 rule is $p = (4, 6, 8, \ldots)$, except if the configuration factor (i.e. integral kernel function) has its first derivative noncontinuous. In such a case, the interval between orders of the Simpson's rule is $q = 0$. Despite the discretization error continuing to reduce after successive extrapolation levels, the order remains 2 at all levels. Thus, in such exceptions, the application of the Simpson's rule has no advantage over the trapezoidal rule. In fact, many configuration factors presented in catalogs [26] are nonpiecewise functions that have their first derivative discontinuous.

7.2. Participating media problems

Frequently the RTE is solved with the DOM, which implies the inclusion of spatial and angular discretization errors. This article presents the error equation to the spatial discretization considering the Finite Volume approach as an *a priori* analysis. After this procedure, one observes if the true order of the error or the error estimate agrees with the prediction. The approach began with a simple problem and gradually increased the complexity of the mathematical model.

The article shows how the two main contributions to spatial discretization error manifest themselves. The first is due to the integration of the intensity with the rectangle rule, which has orders $p = \{3, 5, 7, \ldots\}$ when applied one by one element of volume as the DOM does. The second is due to the weighting average scheme application, written as a function of the weighting factor γ. The step scheme ($\gamma = 1$) has true orders $p = \{1, 2, 3, \ldots\}$ and the diamond scheme ($\gamma = 1/2$) has orders $p = \{2, 4, 6, \ldots\}$.

By combining these three sources of error within the discretization of the RTE as done by the DOM it was possible to show very accurately how these sources of error manifest as the process of marching in space progresses. Despite the simplifications of the RTE, the strategy can be applied to multidimensional problems and, perhaps also to describe the angular discretization error.

When RRE is used to extrapolate numerical results obtained with the DOM, all global variables generally presented orders $p = \{1,\ 2,\ 3,\ \ldots\}$ when using the step scheme and $p = \{2,\ 4,\ 6,\ \ldots\}$ when using the diamond scheme, even when the scattering is considered. The exceptions occur only to the incident radiation and temperature, both measured in the middle of the domain and only when the medium temperature is variable, indicating one more error source in the integration of the RTE source term.

Acknowledgments

The authors would like to thank the reviewers for their observations and contributions to this article. The first author was supported by a CAPES scholarship under the Finance Code 001.

Funding

C. H. Marchi was supported by a CNPq scholarship. L. M. Moura was supported by the CNPq scholarship under Grant number 313994/2021-8.

ORCID

Antonio Carlos Foltran http://orcid.org/0000-0003-4899-5652
Carlos Henrique Marchi http://orcid.org/0000-0002-1195-5377
Luís Mauro Moura http://orcid.org/0000-0003-3837-4895

References

[1] P. Knupp and K. Salari, *Verification of Computer Codes in Computational Science and Engineering*. Boca Raton, FL: Chapman & Hall, 2003.
[2] W. L. Oberkampf and C. J. Roy, *Verification and Validation in Scientific Computing*. Cambridge, UK: Cambridge Univ. Press, 2010,
[3] P. J. Roache, *Fundamentals of Verification and Validation*, 2nd ed. Socorro, NM: Hermosa, 2009.
[4] American Society of Mechanical Engineers. *Standard for Verification and Validation in Computational Fluid Dynamics and Heat Transfer – ASME V&V 20-2009*. New York, NY: American Society of Mechanical Engineers, 2009.
[5] P. J. Coelho, "Advances in the discrete ordinates and finite volume methods for the solution of radiative heat transfer problems in participating media," *J. Quant. Spectrosc. Radiat. Transf.*, vol. 145, pp. 121–146, 2014. DOI: 10.1016/j.jqsrt.2014.04.021.
[6] S. N. Dhurandhar, A. Bansal, S. P. Boppudi, and M. D. M. Kadiyala, "Application and comparative analysis of radiative heat transfer models for coal-fired furnace," *Numer. Heat Tr. A-Appl.*, vol. 82, no. 4, pp. 137–168, 2022. DOI: 10.1080/10407782.2022.2067400.
[7] E. M. Sparrow and R. D. Cess, *Radiation Heat Transfer*, Augmented ed. Washington, DC: Hemisphere, 1978.
[8] P. J. Roache and P. M. Knupp, "Complete Richardson Extrapolation," *Commun. Numer. Meth. Eng.*, vol. 9, no. 5, pp. 365–374, 1993. DOI: 10.1002/cnm.1640090502.
[9] A. Sidi, *Practical Extrapolation Methods – Theory and Applications*. Cambridge, UK: Cambridge University Press, 2003.
[10] C. H. Marchi, R. Suero, and L. K. Araki, "The lid-driven square cavity flow: Numerical solution with a 1024×1024 grid," *J. Braz. Soc. Mech. Sci.*, vol. 31, no. 3, pp. 186–198, 2009. DOI: 10.1590/S1678-58782009000300004.
[11] J. H. Ferziger and M. Perić, *Computational Methods for Fluid Dynamics*, 3rd ed. Berlin, DE: Springer, 2002, p. 58.
[12] C. H. Marchi, L. A. Novak, C. D. Santiago, and A. P. S. Vargas, "Highly accurate numerical solutions with repeated Richardson extrapolation for 2d Laplace equation," *Appl. Math. Model.*, vol. 37, no. 12–13, pp. 7386–7397, 2013. DOI: 10.1016/j.apm.2013.02.043.

[13] B. P. Leonard, “Comparison of truncation error of finite-difference and finite-volume formulations of convection terms,” *Appl. Math. Model.*, vol. 18, no. 1, pp. 46–50, 1994. DOI: 10.1016/0307-904X(94)90182-1.
[14] B. P. Leonard, “Order of accuracy of QUICK and related convection-diffusion schemes,” *Appl. Math. Model.*, vol. 19, no. 11, pp. 640–653, 1995. DOI: 10.1016/0307-904X(94)90182-1.
[15] C. H. Marchi, 2001. “Verification of unidimensional numerical solutions in computational fluid dynamics,” PhD thesis, Graduate Program in Mechanical Engineering, POSMEC, Santa Catarina Federal Univ. Florianópolis, SC, BR (in portuguese).
[16] L. P. da Silva, C. H. Marchi, M. Meneguette, and A. C. Foltran, “Robust RRE technique for increasing the order of accuracy of SPH numerical solutions,” *Math. Comput. Simul.*, vol. 199, pp. 231–252, 2022. DOI: 10.1016/j.matcom.2022.03.016.
[17] A. C. Foltran, C. H. Marchi, and L. M. Moura, “Truncation error for the Simpson’s 1/3 rule based on Taylor series expansion,” 18th Brazilian Congress of Thermal Sciences and Engineering, Nov. 2020, pp. 1–10. DOI: 10.26678/ABCM.ENCIT2020.CIT20-0167.
[18] J. C. Chai, H. S. Lee, and S. V. Patankar, “Ray effect and false scattering in the discrete ordinates method,” *Numer. Heat Tr., B-Fund.*, vol. 24, no. 4, pp. 373–389, 1993. DOI: 10.1080/10407799308955899.
[19] J. P. Jessee and W. A. Fiveland, “Bounded, high resolution differencing schemes applied to the discrete ordinates method,” *J. Thermophys. Heat Trans.*, vol. 11, no. 4, pp. 540–548, 1997. DOI: 10.2514/2.6296.
[20] G. D. Raithby, “Evaluation of discretization errors in finite-volume radiant heat transfer predictions,” *Numer. Heat Tr., B-Fund.*, vol. 36, no. 3, pp. 241–264, 1999. DOI: 10.1080/104077999275631.
[21] E. D. Larsen and A. B. Wollaber, “A quantitative theory of angular truncation errors in 3-D discrete ordinates calculations,” M&C + SNA Topical Meeting, Joint Int. Topical Meeting Mathematics & Computation Supercomputing Nucl. Applications, vol. 1, pp. 287–304, Apr. 2007.
[22] C. H. Marchi and A. F. C. Silva, “Multi-dimensional discretization error estimation for convergent apparent order,” *J. Braz. Soc. Mech. Sci. Eng.*, vol. 27, no. 4, pp. 432–439, 2005. DOI: 10.1590/S1678-58782005000400012.
[23] C. M. Usiskin and R. Siegel, “Thermal radiation from a cylindrical enclosure with specified wall heat flux,” *J. Heat Transf.*, vol. 82, no. 4, pp. 369–374, 1960. DOI: 10.1115/1.3679956.
[24] C. H. Marchi and A. C. Alves, “Verification of numerical solutions of the advection-diffusion and Burgers equations,” *Appl. Comput. Math.*, vol. 3, no. 2, pp. 1–7, 2014. DOI: 10.4172/2168-9679.1000154.
[25] M. A. Heaslet and R. F. Warming, “Radiative transport and wall temperature slip in an absorbing planar medium,” *Int. J. Heat Mass Transf.*, vol. 8, no. 7, pp. 979–994, 1965. DOI: 10.1016/0017-9310(65)90083-9.
[26] J. R. Howell, “A catalog of radiation configuration factors,” Department of Mechanical Engineering, Univ. of Texas, Austin, TX. [Online]. Available: http://www.thermalradiation.net/indexCat.html. Accessed: Oct. 24, 2021.

Appendix A: Deduction of the truncation error due to the weighting average

Given the interval $[x_w, x_e]$, a weighting factor γ is defined by

$$\gamma \equiv \frac{x_\gamma - x_w}{x_e - x_w}, \tag{A1}$$

where x_γ is an arbitrary position as shown by Figure A1. This factor makes the well-known step difference ($\gamma = 1$) and diamond difference ($\gamma = 1/2$) schemes.

It is easy to see that

$$x_w - x_\gamma = -\gamma h, \tag{A2}$$

$$x_e - x_\gamma = (1-\gamma)h. \tag{A3}$$

The deduction of the truncation error in the center of volume $E_{\bar{I},P}$ began expanding the directional intensity in Taylor Series around the point x_γ

$$I(x) = I_{x_\gamma} + I^{i}_{x_\gamma}(x - x_\gamma) + \frac{I^{ii}_{x_\gamma}}{2}(x - x_\gamma)^2 + \frac{I^{iii}_{x_\gamma}}{6}(x - x_\gamma)^3 + \frac{I^{iv}_{x_\gamma}}{24}(x - x_\gamma)^4 + \frac{I^{v}_{x_\gamma}}{120}(x - x_\gamma)^5 + \frac{I^{vi}_{x_\gamma}}{720}(x - x_\gamma)^6 + \ldots \tag{A4}$$

Making $x = x_e$ gives the intensity at the east face I_e

$$I_e = I_{x_\gamma} + I^{i}_{x_\gamma}(1-\gamma)h + \frac{I^{ii}_{x_\gamma}}{2}(1-\gamma)^2h^2 + \frac{I^{iii}_{x_\gamma}}{6}(1-\gamma)^3h^3 + \frac{I^{iv}_{x_\gamma}}{24}(1-\gamma)^4h^4 + \frac{I^{v}_{x_\gamma}}{120}(1-\gamma)^5h^5 + \frac{I^{vi}_{x_\gamma}}{720}(1-\gamma)^6h^6 + \ldots \tag{A5}$$

In the same way, making $x = x_w$ gives the intensity at the west face I_w

$$I_w = I_{x_\gamma} - I^{i}_{x_\gamma}\gamma h + \frac{I^{ii}_{x_\gamma}}{2}\gamma^2h^2 - \frac{I^{iii}_{x_\gamma}}{6}\gamma^3h^3 + \frac{I^{iv}_{x_\gamma}}{24}\gamma^4h^4 - \frac{I^{v}_{x_\gamma}}{120}\gamma^5h^5 + \frac{I^{vi}_{x_\gamma}}{720}\gamma^6h^6 + \ldots \tag{A6}$$

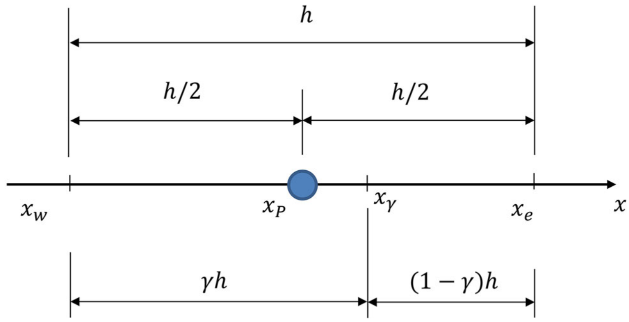

Figure A1. Graphical definition of the weighting factor γ.

The weighting factor γ appears in both Eqs. (A5) and (A6), however, they are written around the point x_γ and the DOM considers the intensity at the volume central point x_P. Therefore, it is necessary to expand the intensity I_{x_γ} around the central point x_P. Considering that $x_\gamma - x_P = (\gamma - 1/2)h$, then the Taylor series around x_P is

$$I_{x_\gamma} = I_P + I_P^i(\gamma-1/2)h + \frac{I_P^{ii}}{2}(\gamma-1/2)^2h^2 + \frac{I_P^{iii}}{6}(\gamma-1/2)^3h^3 + \frac{I_P^{iv}}{24}(\gamma-1/2)^4h^4 + \frac{I_P^{v}}{120}(\gamma-1/2)^5h^5 + \frac{I_P^{vi}}{720}(\gamma-1/2)^6h^6 + \ldots. \tag{A7}$$

The six first derivatives in Eqs. (A5) and (A6) are also required to write around the nodal point x_P. Considering the appropriate number of terms until the sixth order, one can find

$$I_{x_\gamma}^i = I_P^i + I_P^{ii}(\gamma-1/2)h + \frac{I_P^{iii}}{2}(\gamma-1/2)^2h^2 + \frac{I_P^{iv}}{6}(\gamma-1/2)^3h^3 + \frac{I_P^{v}}{24}(\gamma-1/2)^4h^4 + \frac{I_P^{vi}}{120}(\gamma-1/2)^5h^5 + \ldots, \tag{A8}$$

$$I_{x_\gamma}^{ii} = I_P^{ii} + I_P^{iii}(\gamma-1/2)h + \frac{I_P^{iv}}{2}(\gamma-1/2)^2h^2 + \frac{I_P^{v}}{6}(\gamma-1/2)^3h^3 + \frac{I_P^{vi}}{24}(\gamma-1/2)^4h^4 + \ldots, \tag{A9}$$

$$I_{x_\gamma}^{iii} = I_P^{iii} + I_P^{iv}(\gamma-1/2)h + \frac{I_P^{v}}{2}(\gamma-1/2)^2h^2 + \frac{I_P^{vi}}{6}(\gamma-1/2)^3h^3 + \ldots, \tag{A10}$$

$$I_{x_\gamma}^{iv} = I_P^{iv} + I_P^{v}(\gamma-1/2)h + \frac{I_P^{vi}}{2}(\gamma-1/2)^2h^2 + \ldots, \tag{A11}$$

$$I_{x_\gamma}^{v} = I_P^{v} + I_P^{vi}(\gamma-1/2)h + \ldots, \tag{A12}$$

$$I_{x_\gamma}^{vi} = I_P^{vi} + \ldots. \tag{A13}$$

Substitution of Eq. (A7) until Eq. (A13) into Eq. (A5) multiplied by γ and adding it to Eq. (A6) multiplied by $(1-\gamma)$ one can find

$$\begin{aligned}
\gamma I_e + (1-\gamma)I_w = {} & I_P + (\gamma-1/2)I_P^i h + I_P^{ii}\left[\frac{(\gamma-1/2)^2}{2} + \frac{(1-\gamma)^2\gamma}{2} + \frac{(1-\gamma)\gamma^2}{2}\right]h^2 \\
& + I_P^{iii}\left\{\frac{(\gamma-1/2)^3}{6} + (\gamma-1/2)\left[\frac{(1-\gamma)^2\gamma}{2} + \frac{(1-\gamma)\gamma^2}{2}\right] + \frac{(1-\gamma)^3\gamma}{6} - \frac{(1-\gamma)\gamma^3}{6}\right\}h^3 \\
& + I_P^{iv}\left\{\frac{(\gamma-1/2)^4}{24} + \frac{(\gamma-1/2)^2}{2}\left[\frac{(1-\gamma)^2\gamma}{2} + \frac{(1-\gamma)\gamma^2}{2}\right] + (\gamma-1/2)\left[\frac{(1-\gamma)^3\gamma}{6} - \frac{(1-\gamma)\gamma^3}{6}\right]\right. \\
& \left. + \frac{(1-\gamma)^4\gamma}{24} + \frac{(1-\gamma)\gamma^4}{24}\right\}h^4 + I_P^{v}\left\{\frac{(\gamma-1/2)^5}{120} + \frac{(\gamma-1/2)^3}{6}\left[\frac{(1-\gamma)^2\gamma}{2} + \frac{(1-\gamma)\gamma^2}{2}\right]\right. \\
& \left. + \frac{(\gamma-1/2)^2}{2}\left[\frac{(1-\gamma)^3\gamma}{6} - \frac{(1-\gamma)\gamma^3}{6}\right] + (\gamma-1/2)\left[\frac{(1-\gamma)^4\gamma}{24} + \frac{(1-\gamma)\gamma^4}{24}\right] + \frac{(1-\gamma)^5\gamma}{120} - \frac{(1-\gamma)\gamma^5}{120}\right\}h^5 \\
& + I_P^{vi}\left\{\frac{(\gamma-1/2)^6}{720} + \frac{(\gamma-1/2)^4}{24}\left[\frac{(1-\gamma)^2\gamma}{2} + \frac{(1-\gamma)\gamma^2}{2}\right] + \frac{(\gamma-1/2)^3}{6}\left[\frac{(1-\gamma)^3\gamma}{6} - \frac{(1-\gamma)\gamma^3}{6}\right]\right. \\
& \left. + \frac{(\gamma-1/2)^2}{2}\left[\frac{(1-\gamma)^4\gamma}{24} + \frac{(1-\gamma)\gamma^4}{24}\right] + (\gamma-1/2)\left[\frac{(1-\gamma)^5\gamma}{120} - \frac{(1-\gamma)\gamma^5}{120}\right] + \frac{(1-\gamma)^6\gamma}{720} + \frac{(1-\gamma)\gamma^6}{720}\right\}h^6 + \ldots,
\end{aligned} \tag{A14}$$

where the terms on the left-hand side and the first one on the right-hand side constitute the approximation made by the DOM in Eq. (19). All the remaining terms constitute the truncation error due to the weighting process $E_{\bar{I},P}$, as stated by Eq. (20). The truncation error in Eq. (A14) can be written in a more concise way by

$$E_{\bar{I}} = F^1_{(\gamma)} I^i_P h + F^2_{(\gamma)} I^{ii}_P h^2 + F^3_{(\gamma)} I^{iii}_P h^3 + F^4_{(\gamma)} I^{iv}_P h^4 + F^5_{(\gamma)} I^{v}_P h^5 + F^6_{(\gamma)} I^{vi}_P h^6 + \ldots, \tag{A15}$$

where the function $F^n_{(\gamma)}$ of order n is given by the following formula, found by a comparison between Eqs. (A14) and (A15).

$$F^n_{(\gamma)} = \sum_{i=0}^{n} \left\{ \frac{(\gamma - 1/2)^{(n-i)}}{(n-i)!\ i!} \left[(1-\gamma)^i \gamma + (-1)^i (1-\gamma)\gamma^i \right] \right\}, \quad n \geq 1. \tag{A16}$$

Making $\gamma = 1$ in Eq. (A15), the truncation error of the step difference scheme is found

$$E_{\bar{I}} = \frac{I^i_P}{2} h + \frac{I^{ii}_P}{8} h^2 + \frac{I^{iii}_P}{48} h^3 + \frac{I^{iv}_P}{384} h^4 + \frac{I^{v}_P}{3,840} h^5 + \frac{I^{vi}_P}{46,080} h^6 + \ldots, \tag{A17}$$

Making $\gamma = 1/2$ in Eq. (A15), the truncation error of the diamond difference scheme is found

$$E_{\bar{I}} = \frac{I^{ii}_P}{8} h^2 + \frac{I^{iv}_P}{384} h^4 + \frac{I^{vi}_P}{46,080} h^6 + \ldots, \tag{A18}$$

Appendix B: Truncation error due to the single application of the rectangle rule in a discrete interval

The Rectangle Rule or Middle Point Rule can be deduced by expanding the intensity in a Taylor Series around the nodal point x_P and integrating it from the west face x_w to the west face x_e

$$\int_{x_w}^{x_e} I dx = \int_{x_w}^{x_e} \left[I_{x_P} + I^i_{x_P}(x - x_P) + \frac{I^{ii}_{x_P}}{2}(x - x_P)^2 + \frac{I^{iii}_{x_P}}{6}(x - x_P)^3 + \frac{I^{iv}_{x_P}}{24}(x - x_P)^4 + \frac{I^{v}_{x_P}}{120}(x - x_P)^5 + \frac{I^{vi}_{x_P}}{720}(x - x_P)^6 + \ldots \right] dx, \tag{B1}$$

that results in

$$\int_{x_w}^{x_e} I dx = I_P h + \frac{I^{ii}_P}{24} h^3 + \frac{I^{iv}_P}{1,920} h^5 + \frac{I^{vi}_P}{322,560} h^7 + \ldots. \tag{B2}$$

The first term on the right side of Eq. (B2) is the Rectangle Rule, and the following terms constitute its truncation error $E_{RR,P}$.

$$E_{RR,P} = \frac{I^{ii}_P}{24} h^3 + \frac{I^{iv}_P}{1,920} h^5 + \frac{I^{vi}_P}{322,560} h^7 + \ldots, \tag{B3}$$

thus the true orders for the single application of the Rectangle Rule are

$$p_V = 3,\ 5,\ 7,\ \ldots. \tag{B4}$$

It is possible to show that Eq. (B3) lead to true orders $p_V = 2,\ 4,\ 6,\ \ldots$ when the integration extends to the entire domain, although this is not done here because the DOM only applies the rule in a single discrete interval.